53rd IEEE Conference on Decision and Control
December 15-17, 2014. Los Angeles, California, USA

Optimal control of connected vehicle systems

Jin I. Ge and Gábor Orosz

Abstract— **In this paper, linear quadratic tracking (LQT) is used to optimize the control gains for connected cruise control (CCC). We consider a vehicle string where the CCC vehicle at the tail receives position and velocity signals through wireless vehicle-to-vehicle (V2V) communication from other vehicles ahead (that are not equipped with CCC). An optimal feedback law is obtained by minimizing a cost function defined by headway and velocity errors and the acceleration of the CCC vehicle on an infinite horizon. We show that the feedback gains can be obtained recursively as signals from vehicles farther ahead become available, and that the gains decay exponentially with the number of cars between the source of the signal and the CCC vehicle. The effects of the cost function on the head-to-tail string stability are investigated and the robustness against variations in human parameters is tested. The analytical results are verified by numerical simulations.**

I. INTRODUCTION

Connected cruise control (CCC) has been proposed to maintain smooth traffic flow in heterogeneous connected vehicle systems by exploiting vehicle-to-vehicle (V2V) communication [1]. The CCC controller receives information about the motion of multiple vehicles ahead, and actuates the vehicle or assists the driver based on these signals. The influence of connectivity structures, signal types, packet drops, and communication delays on the longitudinal motion of vehicular chains that include CCC vehicles has been investigated [2]–[5]. Our goal here is to optimize the feedback gains in order to maximize the benefit of connectivity and reduce the complexity of tuning gains individually in large systems; see [6], [7] for initial attempts using simple configurations. Moreover, the design parameters should be chosen so that additional performance requirements(such as string stability) are satisfied.

In this paper we optimize the gains of a CCC vehicle that receives position and velocity information from multiple human-driven vehicles ahead. The goal of optimization is to obtain a CCC controller that ensures the stability of uniform traffic flow (i.e. the attenuation of perturbations along the vehicular chain), while minimizing velocity and headway error and acceleration of the CCC vehicle. This problem is solved by using linear quadratic tracking (LQT) with design parameters being the weights on the error terms and the acceleration term in the cost function. We show that the gains of the optimized controller follow the spatial causality of traffic systems: information from vehicles farther downstream have less influence on the CCC vehicle and does not change the feedback laws on signals from closer vehicles. The optimal gains are determined by the weights used in the optimization (design parameters) and the driver parameters of other vehicles. The range of design parameters ensuring head-to-tail string stability, and their robustness against variations of driver parameters are also demonstrated. Finally, simulations are performed to demonstrate the effectiveness of the optimal design.

*This work was supported by the National Science Foundation (Award Number 1351456)

Jin I. Ge and Gábor Orosz are with the Department of Mechanical Engineering, University of Michigan, Ann Arbor, Michigan 48109, USA. Corresponding email: gejin@umich.edu, orosz@umich.edu

II. CONNECTED CAR-FOLLOWING MODELS

We consider a chain of $n+1$ vehicles traveling on a single lane as shown in Fig. 1(a). The tail vehicle (the last vehicle of the chain) implements a CCC algorithm using position and velocity signals received through V2V communication from n preceding vehicles, while other vehicles are human driven and only transmit information about their motion. The dynamics of the CCC vehicle is modeled by

$$\begin{aligned} \dot{h}_1(t) &= v_2(t) - v_1(t)\,, \\ \dot{v}_1(t) &= u(t)\,, \end{aligned} \tag{1}$$

where the dot stands for differentiation with respect to time t, h_1 is the headway (i.e., the bumper-to-bumper distance between the CCC vehicle and the vehicle immediately ahead), and v_1 is the velocity of the CCC vehicle; see Fig. 1(a). Finally, $u(t)$ is the control input that will be designed using LQT based on the velocity and headway of other vehicles (the latter obtained from position information).

For simplicity, we consider that vehicles $i = 2, \dots, n$ are identical and are described by the car-following model

$$\begin{aligned} \dot{h}_i(t) &= v_{i+1}(t) - v_i(t)\,, \\ \dot{v}_i(t) &= \alpha\big(V(h_i(t)) - v_i(t)\big) + \beta\left(v_{i+1}(t) - v_i(t)\right), \end{aligned} \tag{2}$$

that can be obtained as a simplification of the physics-based model presented in [1]. Here h_i and v_i denote the headway and velocity of vehicle i; see Fig. 1(a). The first term in the second equation represents the driver's intention to drive at a distance-dependent velocity (given by $V(h)$), while the second term represents the driver's aim to match the velocity to that of the vehicle immediately ahead. The corresponding gains are denoted α and β. We remark that the proposed algorithm can also be applied in case of non-identical drivers as well.

The desired velocity in (2) is determined by the range policy

$$V(h) = \begin{cases} 0 & \text{if} \quad 0 \le h \le h_{\rm st}\,, \\ \frac{v_{\max}}{2}\left(1 - \cos\left(\pi \frac{h - h_{\rm st}}{h_{\rm go} - h_{\rm st}}\right)\right) & \text{if} \quad h_{\rm st} < h < h_{\rm go}\,, \\ v_{\max} & \text{if} \quad h \ge h_{\rm go}\,, \end{cases} \tag{3}$$

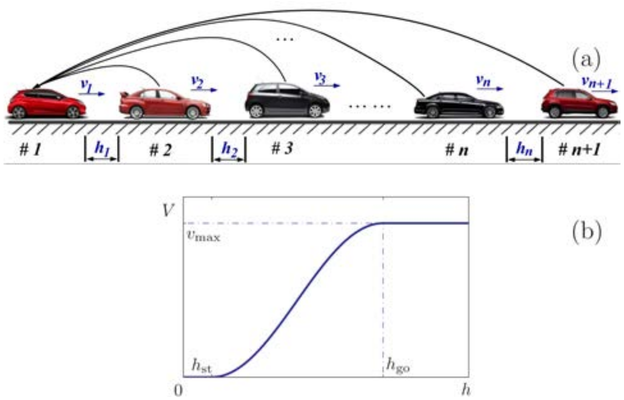

Fig. 1. (a): A chain of $n+1$ vehicles with a CCC vehicle at the tail receiving signals from other vehicles via V2V communication. (b): The nonlinear range policy (3) used in this paper.

which is shown in Fig. 1(b). The desired velocity is zero for small headways ($0 \leq h \leq h_{\rm st}$) and equal to the maximum speed $v_{\max}$ for large headways ($h \geq h_{\rm go}$). Between these, it increases with the headway monotonically. To ensure smooth longitudinal dynamics, the function (3) and its derivative are chosen to be continuous at $h_{\rm st}$ and $h_{\rm go}$. Here we consider $v_{\max} = 30$ [m/s], $h_{\rm st} = 5$ [m], $h_{\rm go} = 35$ [m] that corresponds to realistic traffic data [8]. Many other range policies may be chosen, but the qualitative dynamics remain similar if the above characteristics are kept [2], [9], [10].

We remark that model (1,2,3) may not adequately describe longitudinal dynamics when vehicles are driven near physical limits, e.g., tire force saturation due to emergency braking or severe maneuvering. In this paper we focus on the potentials of wireless connectivity, while understanding such limitations is left for future research.

III. Linear Quadratic Tracking of Uniform Traffic Flow

In this section, the optimal control problem under disturbance is formulated, where the CCC vehicle is tracking the uniform flow state. The cost function is constructed in order to minimize the headway and velocity errors and the acceleration of the CCC vehicle. The solution gives the gains for the CCC vehicle with respect to the headways and velocities of other vehicles.

The dynamics of the connected vehicle system (1,2) is investigated in the vicinity of an equilibrium where all vehicles travel with the same constant velocity and maintain constant headways. While the equilibrium velocity v^* is determined by the head vehicle (the first vehicle in the chain), the equilibrium headway h_i^* is obtained for each non-CCC vehicle using a range policy $v^* = V_i(h_i^*)$, $i = 2, \ldots, n$. When considering identical range policies (cf. (3)), the vehicles are equidistant and we obtain the uniform flow equilibrium

$$h_i(t) \equiv h^*\,, \quad v_i(t) \equiv v^* = V(h^*)\,, \tag{4}$$

for $i = 2, \ldots, n$. We define headway perturbations $\tilde{h}_i(t) = h_i(t) - h^*$ and velocity perturbations $\tilde{v}_i(t) = v_i(t) - v^*$, $i = 2, \ldots, n$, and linearize (2) about the equilibrium (4):

$$\begin{aligned} \dot{\tilde{h}}_i(t) &= \tilde{v}_{i+1}(t) - \tilde{v}_i(t)\,, \\ \dot{\tilde{v}}_i(t) &= \alpha\big(f^*\tilde{h}_i(t) - \tilde{v}_i(t)\big) + \beta\,\dot{\tilde{h}}_i(t)\,, \end{aligned} \tag{5}$$

for $i = 2, \ldots, n$. Here $f^* = V'(h^*)$ is the derivative of the range policy at the equilibrium and the corresponding time headway is $t_{\rm h} = 1/f^*$. In this paper, we use $(h^*, v^*) = (20\,[\rm m], 15\,[\rm m/s])$, which results in the maximum slope $f^* = \pi/2\,[1/\rm s]$ corresponding to the minimum time headway $t_{\rm h} = 2/\pi \approx 0.64$ [s]; cf. (3) with $v_{\max} = 30$ [m/s], $h_{\rm st} = 5$ [m], and $h_{\rm go} = 35$ [m].

For the CCC vehicle, we define headway perturbation $\tilde{h}_1(t) = h_1(t) - h_1^*$ and velocity perturbation $\tilde{v}_1(t) = v_1(t) - v^*$. Then (1) yields the linearized dynamics

$$\begin{aligned} \dot{\tilde{h}}_1(t) &= \tilde{v}_2(t) - \tilde{v}_1(t)\,, \\ \dot{\tilde{v}}_1(t) &= u(t)\,. \end{aligned} \tag{6}$$

Let's define the state $x = [\tilde{h}_1, \tilde{v}_1, \ldots, \tilde{h}_n, \tilde{v}_n]^{\rm T} \in \mathbb{R}^{2n}$, and write dynamics (5,6) in the form

$$\dot{x}(t) = \mathbf{A}x(t) + \mathbf{B}u(t) + \mathbf{D}\tilde{v}_{n+1}(t)\,, \tag{7}$$

where $u(t)$ is the input, $\tilde{v}_{n+1}(t)$ is the disturbance, and the coefficient matrices take the form

$$\mathbf{A} = \begin{bmatrix} \mathbf{A}_1 & \mathbf{A}_2 & & & \\ & \mathbf{A}_3 & \mathbf{A}_4 & & \\ & & \ddots & \ddots & \\ & & & \mathbf{A}_3 & \mathbf{A}_4 \\ & & & & \mathbf{A}_3 \end{bmatrix}, \mathbf{B} = \begin{bmatrix} \mathbf{B}_1 \\ \mathbf{0} \\ \vdots \\ \mathbf{0} \\ \mathbf{0} \end{bmatrix}, \mathbf{D} = \begin{bmatrix} \mathbf{0} \\ \mathbf{0} \\ \vdots \\ \mathbf{0} \\ \mathbf{D}_1 \end{bmatrix} \tag{8}$$

where the block matrices are given by

$$\begin{aligned} &\mathbf{A}_1 = \begin{bmatrix} 0 & -1 \\ 0 & 0 \end{bmatrix},\ \mathbf{A}_2 = \begin{bmatrix} 0 & 1 \\ 0 & 0 \end{bmatrix},\ \mathbf{A}_4 = \begin{bmatrix} 0 & 1 \\ 0 & \beta \end{bmatrix}, \\ &\mathbf{A}_3 = \begin{bmatrix} 0 & -1 \\ \alpha f^* & -\alpha - \beta \end{bmatrix},\ \mathbf{B}_1 = \begin{bmatrix} 0 \\ 1 \end{bmatrix},\ \mathbf{D}_1 = \begin{bmatrix} 1 \\ \beta \end{bmatrix}. \end{aligned} \tag{9}$$

Since our goal is to track the uniform flow equilibrium $x^* \equiv 0$ (cf. (4)) under velocity disturbance $\tilde{v}_{n+1}(t)$ from the head vehicle, we minimize the cost function

$$J_\tau(u, x) = \int_0^\tau \big(x^{\rm T}(t)\mathbf{Q}x(t) + r\,u^2(t)\big)\,{\rm d}t\,. \tag{10}$$

The first term corresponds to the variation of the headways and velocities which we call tracking errors, the second term corresponds to the "magnitude" of the CCC vehicle's acceleration, and τ is the time horizon (we use $\tau \to \infty$ later). The weight matrix $\mathbf{Q}$ is chosen to be diagonal, that is,

$$\mathbf{Q} = {\rm diag}\left([q_1, q_2, \ldots, q_{2n-1}, q_{2n}]\right), \tag{11}$$

where q_{2i-1} and q_{2i} are the weights on the headway and velocity errors for vehicle i, respectively. Since only vehicle 1 has the CCC controller, $\tilde{h}_i$, $\tilde{v}_i$, $i = 2, \ldots, n$ are not controllable and the choice of q_{2i-1}, q_{2i}, $i = 2, \ldots, n$ does not influence the optimal control input. Thus we set $q_{2i-1} = q_{2i} = 0$, $i = 2, \ldots, n$.

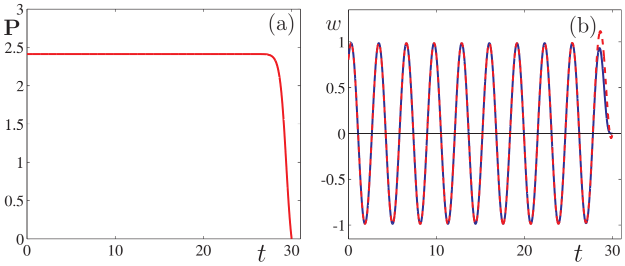

Fig. 2. (a): The solution $\mathbf{P}(t)$ of (13) with $\mathbf{A} = 1, \mathbf{B} = 1, \mathbf{Q} = 1, r = 1, \tau = 30$ [s]. (b): The corresponding solution $w(t)$ of (14) with perturbation $\tilde{v}_{n+1}(t) = \sin(2t)$, using $\mathbf{P}(t)$ shown in panel (a) (red dashed curve) and using the approximation $\mathbf{P} = \mathbf{P}(0)$ (blue solid curve).

Based on the linear quadratic tracking theory [11], the solution of the optimal control problem (7,8,10,11) is given by

$$u(t) = -\frac{1}{r}\mathbf{B}^{\mathrm{T}}\big(\mathbf{P}(t)x(t) + w(t)\big)\,, \tag{12}$$

where $\mathbf{P}(t) \in \mathbb{R}^{2n\times 2n}$ is a symmetric, positive definite matrix that satisfies the Riccati differential equation

$$\dot{\mathbf{P}}(t) = \frac{1}{r}\mathbf{P}(t)\mathbf{B}\mathbf{B}^{\mathrm{T}}\mathbf{P}(t) - \mathbf{A}^{\mathrm{T}}\mathbf{P}(t) - \mathbf{P}(t)\mathbf{A} - \mathbf{Q}\,, \tag{13}$$

with end boundary condition $\mathbf{P}(\tau) = \mathbf{0}$, while $w(t) \in \mathbb{R}^{2n}$ is the solution of

$$\dot{w}(t) = -\Big(\mathbf{A} - \frac{1}{r}\mathbf{B}\mathbf{B}^{\mathrm{T}}\mathbf{P}(t)\Big)^{\mathrm{T}} w(t) - \mathbf{P}(t)\mathbf{D}\tilde{v}_{n+1}(t)\,, \tag{14}$$

with end boundary condition $w(\tau) = 0$. Note that without disturbance, i.e., $\tilde{v}_{n+1}(t) \equiv 0$, the LQT problem (7,10) simplifies to an LQR problem with input $u(t) = -\frac{1}{r}\mathbf{B}^{\mathrm{T}}\mathbf{P}(t)x(t)$, where $\mathbf{P}(t)$ is the solution of (13).

According to [11], when the system (7,8) is stabilizable, then (13) has uniformly bounded solution. Moreover, in the infinite-time horizon $\tau \to \infty$, the solution $\mathbf{P}(t)$ can be approximated by a constant matrix given by the algebraic Riccati equation

$$\mathbf{A}^{\mathrm{T}}\mathbf{P} + \mathbf{P}\mathbf{A} + \mathbf{Q} - \frac{1}{r}\mathbf{P}\mathbf{B}\mathbf{B}^{\mathrm{T}}\mathbf{P} = 0\,. \tag{15}$$

From now on we use $\mathbf{P}$ without t to denote this time-independent matrix. Substituting $\mathbf{P}$ into (14), and considering that $(\mathbf{A} - \frac{1}{r}\mathbf{B}\mathbf{B}^{\mathrm{T}}\mathbf{P})$ is Hurwitz, the boundary value problem can be viewed as an initial value problem with a special initial condition that eliminates the transients. A simple example is given in Fig. 2 for the simplified problem $\dot{x}(t) = x(t) + u(t) + \tilde{v}_{n+1}(t)$, $x, u \in \mathbb{R}$ using the weights $\mathbf{Q} = 1$, $r = 1$. Panel (a) shows that $\mathbf{P}(t)$ is approximately constant when $t \ll \tau$. Panel (b) shows that using constant $\mathbf{P} = \mathbf{P}(0)$ instead of $\mathbf{P}(t)$ in (14) only influences $w(t)$ near time τ. Thus for large τ, $\mathbf{P}(t)$ can be approximated by $\mathbf{P} = \mathbf{P}(0)$ and the latter can be used to calculate $w(t)$.

Let us define the notation

$$\mathbf{P} = \begin{bmatrix} \mathbf{\Pi}_{11} & \dots & \mathbf{\Pi}_{1n} \\ \vdots & \ddots & \vdots \\ \mathbf{\Pi}_{n1} & \dots & \mathbf{\Pi}_{nn} \end{bmatrix}, \tag{16}$$

where $\mathbf{\Pi}_{ij} = \mathbf{\Pi}_{ji}^{\mathrm{T}} \in \mathbb{R}^{2\times 2}$, $i,j = 1,\dots,n$. Considering infinite time horizon $\tau \to \infty$, the feedback law (12) gives the acceleration of the CCC vehicle in (6) as

$$u(t) = \sum_{i=1}^{n}\big(\alpha_i\,\tilde{h}_i(t) + \beta_i\,\tilde{v}_i(t)\big) - \frac{1}{r}w_2(t)\,, \tag{17}$$

where $w_2(t)$ denotes the second element of $w(t)$ and the gains α_i and β_i are given by

$$\alpha_i = -\frac{1}{r}\mathbf{\Pi}_{1i}[2,1]\,, \quad \beta_i = -\frac{1}{r}\mathbf{\Pi}_{1i}[2,2]\,, \tag{18}$$

for $i = 1,\dots,n$, where $[k,l]$ represents the element in the k^{th} row and l^{th} column.

Due to the particular form of the coefficient matrices (8), for $i = j = 1$, (15) yields

$$\mathbf{\Pi}_{11}\tilde{\mathbf{B}}_1\mathbf{\Pi}_{11} - \mathbf{\Pi}_{11}\mathbf{A}_1 - \mathbf{A}_1^{\mathrm{T}}\mathbf{\Pi}_{11} - \mathrm{diag}([q_1, q_2]) = \mathbf{0}\,, \tag{19}$$

where $\tilde{\mathbf{B}}_1 = \frac{1}{r}\mathbf{B}_1\mathbf{B}_1^{\mathrm{T}}$; c.f. (9). Moreover, using (15) it can be shown that the first row of block matrices in $\mathbf{P}$ (cf. (16)) satisfy the recursive equations

$$\begin{aligned} &\big(\mathbf{A}_1^{\mathrm{T}} - \mathbf{\Pi}_{11}\tilde{\mathbf{B}}_1\big)\mathbf{\Pi}_{12} + \mathbf{\Pi}_{12}\mathbf{A}_3 = -\mathbf{\Pi}_{11}\mathbf{A}_2\,, \\ &\big(\mathbf{A}_1^{\mathrm{T}} - \mathbf{\Pi}_{11}\tilde{\mathbf{B}}_1\big)\mathbf{\Pi}_{1j} + \mathbf{\Pi}_{1j}\mathbf{A}_3 = -\mathbf{\Pi}_{1(j-1)}\mathbf{A}_4\,, \end{aligned} \tag{20}$$

where $j = 3,\dots,n$. Also, the second row of block matrices satisfy the recursive equations

$$\begin{aligned} &\mathbf{A}_3^{\mathrm{T}}\mathbf{\Pi}_{22} + \mathbf{\Pi}_{22}\mathbf{A}_3 = \mathbf{\Pi}_{21}\tilde{\mathbf{B}}_1\mathbf{\Pi}_{12} - \mathbf{\Pi}_{12}^{\mathrm{T}}\mathbf{A}_2 - \mathbf{A}_2^{\mathrm{T}}\mathbf{\Pi}_{12}\,, \\ &\mathbf{A}_3^{\mathrm{T}}\mathbf{\Pi}_{2j} + \mathbf{\Pi}_{2j}\mathbf{A}_3 = \mathbf{\Pi}_{21}\tilde{\mathbf{B}}_1\mathbf{\Pi}_{1j} - \mathbf{\Pi}_{2(j-1)}\mathbf{A}_4 - \mathbf{A}_2^{\mathrm{T}}\mathbf{\Pi}_{1j}\,, \end{aligned} \tag{21}$$

where $j = 3,\dots,n$ and $\mathbf{\Pi}_{21} = \mathbf{\Pi}_{12}^{\mathrm{T}}$. For the remaining $n-2$ rows of block matrices, we obtain the recursive equations

$$\mathbf{A}_3^{\mathrm{T}}\mathbf{\Pi}_{ij} + \mathbf{\Pi}_{ij}\mathbf{A}_3 = \mathbf{\Pi}_{i1}\tilde{\mathbf{B}}_1\mathbf{\Pi}_{1j} - \mathbf{\Pi}_{i(j-1)}\mathbf{A}_4 - \mathbf{A}_4^{\mathrm{T}}\mathbf{\Pi}_{(i-1)j}\,, \tag{22}$$

where $i = 3,\dots,n$, $j = i,\dots,n$ and $\mathbf{\Pi}_{i1} = \mathbf{\Pi}_{1i}^{\mathrm{T}}$. Thus, the solution of the Riccati equation (15) can be obtained by solving (19,20,21,22) consecutively.

In the physically realistic case $q_1, q_2, r > 0$, the only feasible solution of (19) is given by

$$\mathbf{\Pi}_{11} = \begin{bmatrix} \sqrt{q_1 q_2 + 2\sqrt{q_1^3 r}} & -\sqrt{q_1 r} \\ -\sqrt{q_1 r} & \sqrt{q_2 r + 2\sqrt{q_1 r^3}} \end{bmatrix}, \tag{23}$$

and thus (18) yields

$$\alpha_1 = \sqrt{q_1/r}, \quad \beta_1 = -\sqrt{q_2/r + 2\sqrt{q_1/r}}\,. \tag{24}$$

Moreover, according to (18), the gains α_i, β_i obtained from (20) can be rewritten as

$$\begin{aligned} &\mathrm{vec}(\mathbf{\Pi}_{12}) = \mathbf{M}_0\mathrm{vec}(\mathbf{\Pi}_{11}), \\ &\mathrm{vec}(\mathbf{\Pi}_{1i}) = \mathbf{M}\mathrm{vec}(\mathbf{\Pi}_{1(i-1)}), \end{aligned} \tag{25}$$

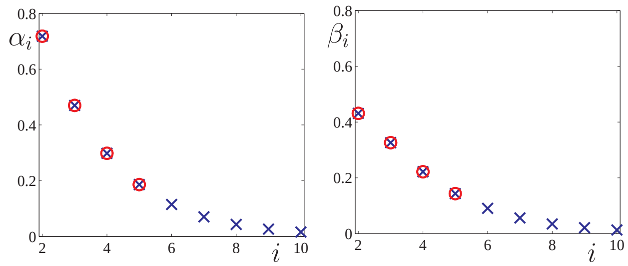

Fig. 3. The optimized headway and velocity gains $\alpha_i, \beta_i, i = 2, \ldots, n$ of the CCC vehicle in a $(n+1)$-car platoon for $n = 5$ (red circles) and for $n = 10$ (blue crosses).

where $\mathrm{vec}(\mathbf{\Pi}_{1i})$, $i = 3, \ldots, n$, is a vector obtained by writing columns of $\mathbf{\Pi}_{1i}$ into a vector and we have

$$\begin{aligned}\mathbf{M} &= -\Big(\mathbf{I} \otimes \big(\mathbf{A}_1^{\mathrm{T}} - \mathbf{\Pi}_{11}\tilde{\mathbf{B}}_1\big) + \mathbf{A}_3^{\mathrm{T}} \otimes \mathbf{I}\Big)^{-1}(\mathbf{A}_4^{\mathrm{T}} \otimes \mathbf{I}),\\ \mathbf{M}_0 &= -\Big(\mathbf{I} \otimes \big(\mathbf{A}_1^{\mathrm{T}} - \mathbf{\Pi}_{11}\tilde{\mathbf{B}}_1\big) + \mathbf{A}_3^{\mathrm{T}} \otimes \mathbf{I}\Big)^{-1}(\mathbf{A}_2^{\mathrm{T}} \otimes \mathbf{I})\,.\end{aligned} \tag{26}$$

Therefore,

$$\mathrm{vec}(\mathbf{\Pi}_{1i}) = \mathbf{M}^{i-2}\mathbf{M_0}\mathrm{vec}(\mathbf{\Pi}_{11}) \tag{27}$$

is a map between $\mathbf{\Pi}_{11}$ and $\mathbf{\Pi}_{1i}$, for $i = 2, \ldots, n$, and thus α_i, β_i, $i = 2, \ldots, n$ can be obtained as functions of $\alpha_1, \beta_1, \alpha, \beta, f^*$; cf. (9,18,26). Moreover, (27) indicates that the feedback gains of vehicle i are determined by the car-following dynamics of vehicles $1, 2, \ldots, i-1$ and are not influenced by the dynamics of vehicles $i+1, \ldots, n+1$. This property means that our CCC design is scalable, since the values of gains can be kept constant regardless how many vehicles ahead are monitored. Finally, we note that (21,22) are only needed to obtain $w(t)$; cf. (14).

One may show that the eigenvalues of $\mathbf{M}$ in (27) are inside the unit circle for human gains $\alpha > 0$, $\beta > 0$. Therefore, (27) is a contracting map in realistic scenarios and α_i and β_i converge to zero following geometric series as i increases. This indicates that the CCC vehicle relies more on signals obtained from closer vehicles, and this characteristic behavior is not influenced by the choice of weights q_1 and q_2 in the cost function (10,11).

As an example, we consider $q_1 = 2\,[1/\mathrm{s}^2]$, $q_2 = 4$, $r = 1\,[\mathrm{s}^2]$ and assume non-CCC vehicles with gains $\alpha = 0.6\,[1/\mathrm{s}]$ and $\beta = 0.9\,[1/\mathrm{s}]$. In this case (24) gives the gains $\alpha_1 \approx 1.41\,[1/\mathrm{s}^2]$, $\beta_1 \approx -2.61\,[1/\mathrm{s}]$. The exponential decay of the gains α_i, β_i with the vehicle index $i = 2, \ldots, n$ is demonstrated graphically in Fig. 3 for a $(5+1)$ vehicle chain (red circles) and for a $(10+1)$ vehicle chain (blue crosses). This is supported by the fact that the eigenvalues of $\mathbf{M}$ in (27) are $\lambda_1 = 0.61$, $\lambda_2 = 0.37$ and $\lambda_{3,4} = 0$, which are located inside the unit circle. We remark that the gains on signals for vehicles 7–10 are small, indicating that close-to-optimal design can be obtained when only observing approximately 5–6 vehicles ahead. In this sense, the benefits of increasing the number of cars ahead saturate, and having very long connections may not be favorable as they only make the network structure more complicated.

IV. Head-to-tail String Stability

In this section, we discuss how the optimal CCC design influences the longitudinal stability of the connected vehicle system. In particular, we analyze plant stability and string stability.

The plant stability of a CCC vehicle is given as follows: suppose that the vehicles whose signals are used by a CCC vehicle are driven at the same constant velocity, then the velocity of the CCC vehicle approaches this constant velocity. String stability characterizes the attenuation of velocity fluctuations as they propagate upstream [12]. However, string stability can only be ensured for the CCC vehicle (as we have no control over the non-CCC vehicles). Therefore, we evaluate the head-to-tail string stability, i.e., compare the velocity fluctuations of the head vehicle and the CCC vehicle at the tail. Notice that this definition allows that vehicles in the middle may amplify the velocity fluctuations of vehicles ahead. Despite the presence of such intra-platoon string instability, a CCC vehicle can be used to ensure head-to-tail string stability.

We consider the velocity perturbation $\tilde{v}_{n+1}$ of the head vehicle as the input and the velocity perturbation $\tilde{v}_1$ of the tail vehicle as the output. Since perturbation signals can be represented using Fourier components and superposition holds for linear systems, the head-to-tail string stability is ensured when sinusoidal signals are attenuated between the head and the tail vehicles for all excitation frequencies. Thus, we consider the periodic excitation $\tilde{v}_{n+1}(t) = v^{\mathrm{amp}}\sin(\omega t)$ and steady-state solution of (7,12,14,15), see Fig. 2(b) for illustration.

Then taking the Laplace transform of (14) with zero initial condition and reversed time while using $\mathbf{P}(t) \equiv \mathbf{P}$ leads to

$$W(s) = (s\mathbf{I} - \mathbf{A} + \frac{1}{r}\mathbf{B}\mathbf{B}^{\mathrm{T}}\mathbf{P})^{-\mathrm{T}}\mathbf{P}\mathbf{D}\tilde{V}_{n+1}(s)\,, \tag{28}$$

where $W(s)$ is the Laplace transform of $w(t)$, $\tilde{V}_{n+1}(s)$ is the Laplace transform of $\tilde{v}_{n+1}(t)$.

Taking the Laplace transform of the system (7,12) with zero initial conditions and eliminating the velocities of the other vehicles and the headways, we obtain the head-to-tail transfer function

$$\begin{aligned}\Gamma(s) = \frac{\tilde{V}_1(s)}{\tilde{V}_{n+1}(s)} &= \frac{1}{G_1(s)}\Big(\alpha_1\Gamma_0^{n-1}(s) + \frac{sF_{n+1}(s)}{G_1(s)}\\ &+ \sum_{i=2}^{n}\big(\alpha_i + (\beta_i s - \alpha_i)\Gamma_0(s)\big)\Gamma_0^{n-i}(s)\Big)\,.\end{aligned} \tag{29}$$

Here $\tilde{V}_1(s)$ and $\tilde{V}_{n+1}(s)$ denote the Laplace transform of $\tilde{v}_1(t)$ and $\tilde{v}_{n+1}(t)$, respectively, and

$$\begin{aligned}&\Gamma_0(s) = \frac{F_0(s)}{G_0(s)}\,, \quad G_0(s) = s^2 + (\alpha+\beta)s + \alpha f^*\\ &F_0(s) = \beta s + \alpha f^*\,, \; G_1(s) = s^2 - \beta_1 s + \alpha_1,\\ &F_{n+1}(s) = (\alpha_n + \beta\beta_n)s + \mathbf{\Pi}_{1n}[1,1] + \beta\mathbf{\Pi}_{1n}[1,2]\,.\end{aligned} \tag{30}$$

Plant stability at the linear level is determined by the denominator of the transfer function in (29). The system

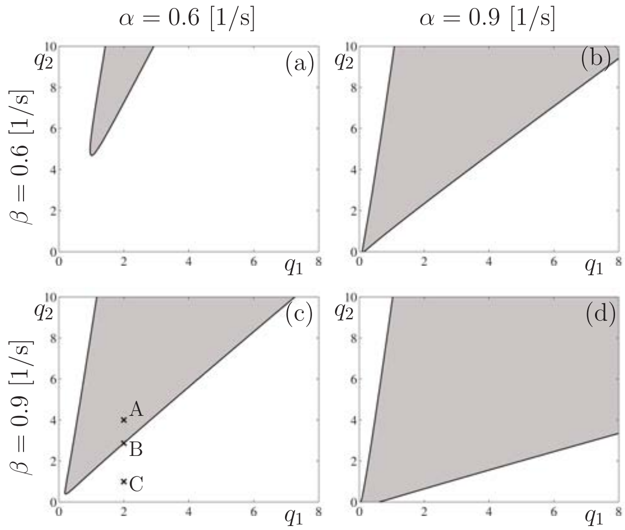

Fig. 4. String stability charts of a $(5+1)$-car platoon in the (q_1, q_2)-plane for different human parameters α, β as indicated. The string stable domains are shaded.

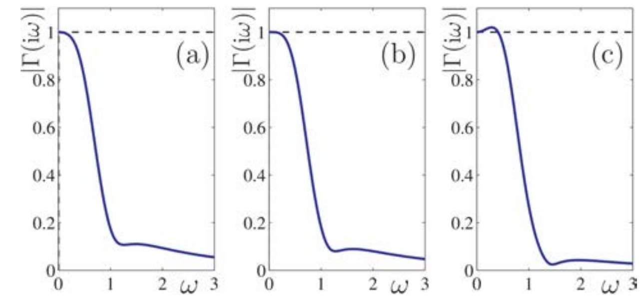

Fig. 5. Magnitude of transfer function as a function of the excitation frequency. Panels (a–c) correspond to points marked A–C in Fig. 4 (c).

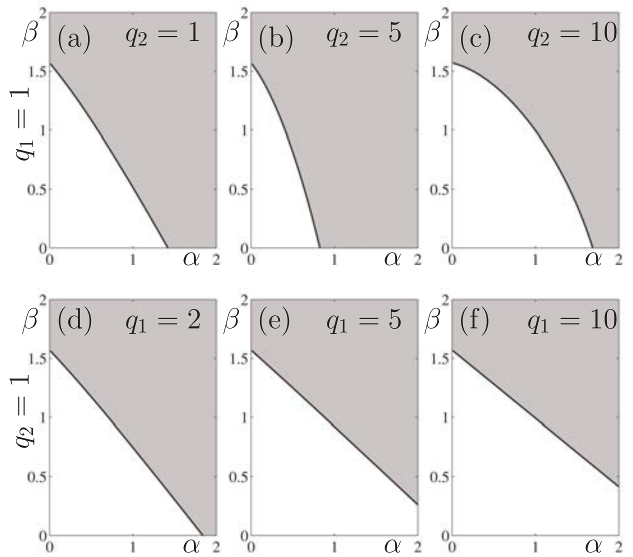

Fig. 6. String stability charts of a $(5+1)$-car platoon in the (α, β)-plane. The notation is the same as in Fig. 4.

is linearly plant stable, if and only if all solutions of the characteristic equation $G_0^n(s)G_1(s) = 0$ are located in the left half complex plane. Notice that plant stability is only influenced by the human parameters α, β and the CCC gains α_1, β_1. Using Routh-Hurwitz criteria, we obtain the conditions for plant stability

$$\alpha > 0\,, \quad \alpha + \beta > 0\,, \quad \alpha_1 > 0\,, \quad \beta_1 < 0\,. \tag{31}$$

In the following analysis, we only consider plant stable human parameters α, β. Solution (23) provides the gains α_1, β_1 that have to satisfy (31). These can be used to obtain all other gains α_i and β_i, $i = 2, \ldots, n$; see (18,27).

At the linear level the necessary and sufficient condition of head-to-tail string stability is given by

$$|\Gamma(\mathrm{i}\omega)|^2 - 1 = \omega^2 f(\omega) < 0\,, \quad \forall \omega > 0\,, \tag{32}$$

where $\Gamma(\mathrm{i}\omega)$ is defined by (29,30); see [4], [13]. The order of $f(\omega)$ increases with the number of vehicles n. String stability is violated when the maximum of $f(\omega)$ is larger than 0, and thus, the string stability boundary is given by the equations

$$f(\omega^{\rm cr}) = 0\,, \quad \frac{\partial f(\omega^{\rm cr})}{\partial \omega} = 0\,, \tag{33}$$

subject to $\dfrac{\partial^2 f(\omega^{\rm cr})}{\partial \omega^2} < 0$, where $\omega^{\rm cr}$ indicates the location of the maximum of $f(\omega)$. To obtain string stability charts, we solve (33) numerically and plot the string stability boundary in the (q_1, q_2)-plane and in the (α, β)-plane. Note that in practical ranges of human parameters α and β the string instability only occurs at zero frequency (i.e., $\omega^{\rm cr} = 0$).

When the human parameters α and β change, the range of weights q_1, q_2, r that results in a string stability changes. Without loss of generality, we fix $r = 1\,[\mathrm{s}^2]$ and only consider the change of weights q_1, q_2. As observed in the previous section, gains on vehicles i, $i > 6$, are small, and therefore we consider $n = 5$.

In Fig. 4 we fix the human parameters $\alpha = 0.6, 0.9\,[1/\mathrm{s}]$ and $\beta = 0.6, 0.9\,[1/\mathrm{s}]$ and shade the string stable domains in the (q_1, q_2)-plane. It has been shown [3] that without CCC, the system is string unstable when

$$\alpha + 2\beta - 2f^* > 0\,, \tag{34}$$

and thus, we have a string unstable system for $q_1 = q_2 = 0$. Fig. 4(a) shows that increasing the weights q_1, q_2 on tracking errors is beneficial for string stability, and that no string stability exists for $q_1 \lesssim 1$, $q_2 \lesssim 4$. However, q_1 and q_2 cannot be chosen independently. Similar results are observed in panels (b–d). Comparing the four panels, one can notice that increasing either α or β increases the size of the string stable domain, while the minimum q_2 ensuring string stability decreases to zero. However, for $q_2 = 0$ the range of string stable q_1 is very small.

We remark that string stability loss in the connected vehicle system analyzed here only happens at zero frequency. Fig. 5 demonstrates such stability loss for the points A–C marked in Fig. 4(c). As q_2 decreases, the magnitude of transfer function (29) increases and it exceeds 1 in the low-frequency domain in case C.

The robustness of optimized CCC designs is investigated by varying the human parameters α and β and the results are summarized in Fig. 6. We fix $q_1 = 1\,[1/\mathrm{s}^2]$ in panels (a–c) and $q_2 = 1$ in panels (d–f), and shade the string stable domains. Increasing α and β improves string stability in each case. For fixed q_1, increasing q_2 enlarges the string stabile area (cf. panels (a) and (b)), but too large q_2 results in smaller string stability region (cf. panels (b) and (c)). For fixed q_2, string stability increases with larger q_1; see (d–f). We remark that string stability may be lost when increasing q_1 even further, although $q_1 < 10$ is considered to be physically realistic. Thus weighting heavily on either h_1 or v_1 is detrimental for string stability.

Finally, to evaluate the performance of our CCC algorithm, we consider a $(5+1)$-car system with string unstable human parameters and investigate the evolution of headway and velocity errors by numerical simulations. Fig. 7 shows the simulation results of the $(5+1)$-car system with gains generated using different design parameters q_1 and q_2. The simulation results are presented for the parameters corresponding to points A and C in Fig. 4(c), while using the disturbance signal $\tilde{v}_{n+1}(t) = v^{\mathrm{amp}} \sin(\omega t)$ with amplitude $v^{\mathrm{amp}} = 1$ [m/s] and frequency $\omega = 0.3$ [rad/s]; see Fig. 5(a,c) for the amplification plots. The simulation results demonstrate that case A is head-to-tail string stable, as the CCC vehicle's velocity fluctuation (thick blue curve) has smaller amplitude than the velocity input (dashed curve) in Fig. 7(a). On the other hand, the CCC vehicle's velocity fluctuation in Fig. 7(c) has larger amplitude than the velocity input, indicating string instability. Note that in both cases the amplitude of velocity fluctuations are amplified by non-CCC vehicles, because the human parameters $\alpha = 0.6\,[1/\mathrm{s}]$, $\beta = 0.9\,[1/\mathrm{s}]$ are string unstable; see (34). Still, the CCC vehicle is able to maintain string stability when q_1, q_2 are chosen appropriately. On the other hand, the comparison of panels (b) and (d) shows a trade-off. While an increased weight on velocity error q_2 ensures string stability, the relative weight on q_1 decreases, and the headway error increases (though still attenuated compared to head vehicle).

V. Conclusion

In this paper, we proposed a connected cruise control design based on linear quadratic tracking and analyzed the head-to-tail string stability. It was shown that the gains depend on the human parameters and the design parameters in the cost function. We found that the optimal gains on preceding vehicles are not influenced by dynamics of vehicles farther downstream, and that the gains decrease with the number of cars between the CCC vehicle and the signaling vehicle. The optimized CCC is shown to be able to stabilize an otherwise string unstable systems when the weights on the headway and velocity errors are chosen appropriately. The design was robust against variations of human parameters, and the results were verified using numerical simulations. Future research includes optimizing nonlinear CCC algorithms while considering more complicated connectivity structures and imperfect communication.

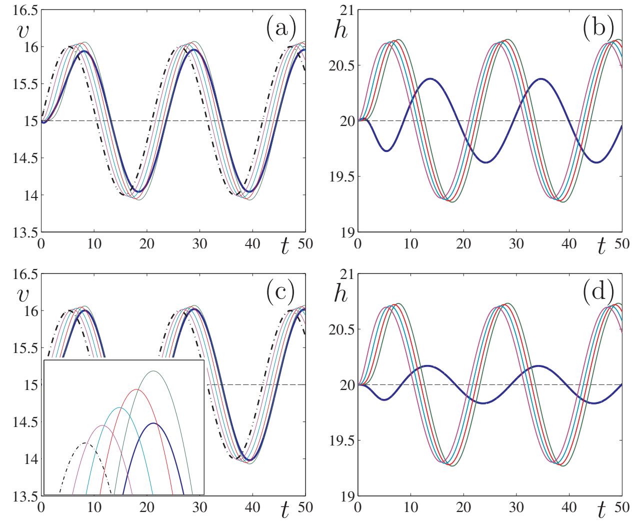

Fig. 7. Velocity and headway responses of a $(5+1)$-car vehicle string with human parameters $\alpha = 0.6\,[1/\mathrm{s}]$, $\beta = 0.9\,[1/\mathrm{s}]$. (a,b): using design parameters $q_1 = 2\,[1/\mathrm{s}^2]$, $q_2 = 4$. (c,d): using design parameters $q_1 = 2\,[1/\mathrm{s}^2]$, $q_2 = 1$. Thick curves denote the CCC vehicle, thin curves are used for non-CCC vehicles, while dashed curves indicate the velocity disturbance of the head vehicle.

References

[1] G. Orosz, "Connected cruise control: modeling, delay effects, and nonlinear behavior," *Vehicle System Dynamics*, p. submitted, 2014.

[2] G. Orosz, R. E. Wilson, and G. Stépán, "Traffic jams: dynamics and control," *Philosophical Transactions of the Royal Society A*, vol. 368, no. 1928, pp. 4455–4479, 2010.

[3] L. Zhang and G. Orosz, "Designing network motifs in connected vehicle systems: delay effects and stability," in *Proceedings of the ASME Dynamical Systems and Control Conference*. ASME, 2013.

[4] J. I. Ge and G. Orosz, "Dynamics of connected vehicle systems with delayed acceleration feedback," *Transportation Research Part C: Emerging Technologies*, vol. 46, pp. 46–64, 2014.

[5] W. B. Qin, M. M. Gomez, and G. Orosz, "Stability analysis of autonomous cruise control with stochastic delay," in *Proceedings of American Control Conference*, 2014.

[6] J. Ploeg, D. Shukla, N. van de Wouw, and H. Nijmeijer, "Controller synthesis for string stability of vehicle platoons," *IEEE Transactions on Intelligent Transportation Systems*, vol. 15, no. 2, pp. 845–865, 2014.

[7] M. Wang, W. Daamen, S. P. Hoogendoorn, and B. van Arem, "Rolling horizon control framework for driver assistance systems. part II: Cooperative sensing and cooperative control," *Transportation Research Part C: Emerging Technologies*, vol. 40, pp. 290 – 311, 2014.

[8] B. S. Kerner, *The Physics of Traffic*. Springer, 2004.

[9] D. C. Gazis, R. Herman, and R. B. Potts, "Car-following theory of steadystate traffic flow," *Operations Research*, vol. 7, no. 4, pp. 499–505, 1959.

[10] A. D. May, *Traffic flow fundamentals*. Prentice Hall, 1990.

[11] E. D. Sontag, *Mathematical Control Theory: Deterministic Finite Dimensional Systems*. Springer, 1998.

[12] P. Seiler, A. Pant, and K. Hedrick, "Disturbance propagation in vehicle strings," *Automatic Control, IEEE Transactions on*, vol. 49, no. 10, pp. 1835–1842, 2004.

[13] L. Zhang and G. Orosz, "Motif-based analysis of connected vehicle systems: delay effects and stability," *Automatica*, p. submitted, 2014.